Journal of Statistical Mechanics:
Theory and Experiment

SISSA

NESMCQ18

Nonstationary distributions and relaxation times in a stochastic model of memristor

To cite this article: N V Agudov *et al J. Stat. Mech.* (2020) 024003

View the article online for updates and enhancements.

IOP ebooks™

Bringing together innovative digital publishing with leading authors from the global scientific community.

Start exploring the collection–download the first chapter of every title for free.

This content was downloaded from IP address 147.163.1.85 on 03/04/2020 at 14:54

Journal of Statistical Mechanics: Theory and Experiment
An IOP and SISSA journal

Nonstationary distributions and relaxation times in a stochastic model of memristor

N V Agudov[1], A V Safonov[1], A V Krichigin[1], A A Kharcheva[1,2], A A Dubkov[1], D Valenti[2,3], D V Guseinov[1], A I Belov[1], A N Mikhaylov[1], A Carollo[1,2] and B Spagnolo[1,2,4]

[1] Laboratory for Stochastic Multistable Systems, Lobachevsky State University, Gagarin ave. 23, 603950 Nizhni Novgorod, Russia
[2] Dipartimento di Fisica e Chimica “Emilio Segrè”, Group of Interdisciplinary Theoretical Physics, Università di Palermo and CNISM, Unità di Palermo, Viale delle Scienze, Edificio 18, I-90128 Palermo, Italy
[3] CNR-IRIB, Consiglio Nazionale delle Ricerche, Istituto per la Ricerca e l'Innovazione Biomedica, Via Ugo La Malfa 153, I-90146, Palermo, Italy
[4] Istituto Nazionale di Fisica Nucleare, Sezione di Catania, Via S. Sofia 64, 95123 Catania, Italy

E-mail: agudov22@gmail.com, dubkov@rf.unn.ru, bernardo.spagnolo@unipa.it and davide.valenti@unipa.it

Received 17 September 2019
Accepted for publication 4 December 2019
Published 19 February 2020

Online at stacks.iop.org/JSTAT/2020/024003
https://doi.org/10.1088/1742-5468/ab684a

Abstract. We propose a stochastic model for a memristive system by generalizing known approaches and experimental results. We validate our theoretical model by experiments carried out on a memristive device based on $Au/Ta/ZrO_2(Y)/Ta_2O_5/TiN/Ti$ multilayer structure. In the framework of the proposed model we obtain the exact analytic expressions for stationary and nonstationary solutions. We analyze the equilibrium and non-equilibrium steady-state distributions of the internal state variable of the memristive system and study the influence of fluctuations on the resistive switching, including the relaxation time to the steady-state. The relaxation time shows a nonmonotonic dependence, with a minimum, on the intensity of the fluctuations. This paves the way for using the intensity of fluctuations as a control parameter for switching dynamics in memristive devices.

© 2020 IOP Publishing Ltd and SISSA Medialab srl
1742-5468/20/024003+23$33.00

Keywords: Brownian motion, defects, diffusion, exact results

Contents

1. Introduction 2

2. Description of the generalized stochastic model 5

3. Comparison with experiment 9

4. Exact solution and analysis 12

5. Conclusions 20

Acknowledgments ... 20

References 21

1. Introduction

Memristors are elements of electric circuits able to change resistance depending on the applied electrical stimulation. These devices attract nowadays great attention as one of the most prospective candidates for next-generation nonvolatile random access memory. This is due to its excellent size scalability down to nanometers, fast switching, low power, and simple structure [1–14]. Within the context of nanotechnologies, production of nanostructures by diffusion is a subject largely investigated [15–17]. Meanwhile, the observed stochasticity in many experiments has emerged as an important inherent property of memristors. Intrinsic stochasticity appears as significant fluctuations in values of cycle-to-cycle resistance levels and lack of predictability in response to the driving electric pulses leading to insufficient read margin between the programmed resistance states. This fact has been perceived across a range of nonvolatile memory technologies such as phase-change memory [18, 19], resistive random access memory [20, 21], electrochemical metallization memory [22], conductive bridge random access memory [23], and among oxide-based memristive materials [9, 24–26]. On the other hand, the non-deterministic behavior of circuit elements is the common feature of nanoelectronics and gives the ground for the newly established field of study named as stochastic electronics [27, 28]. With extensive miniaturization, the circuit elements are increasingly diverting away from their deterministic behavior and the fluctuation level, which in classical theory has been considered as a small disturbing factor, cannot be neglected at nanoscales [29]. This stochastic operation highly mimics the biological medium within the brain. Therefore, using memristor as a basic element of future neural computers looks to be even more promising [9, 30–35]. This paper is dedicated to the investigation of the basic model for stochasticity of memristors and thereby it provides the ground for understanding how the intrinsic fluctuations can represent a drawback or a benefit for emerging applications.

By stochasticity of a memristive system we mean the inherent fluctuations in structure, chemistry, physical values and switching times, which can occur over multiple lengths and time scales during the switching events. For investigating the properties of this stochasticity and understanding how it influences the system it is important to construct the appropriate theoretical model [36]. This model should catch the fundamental balance laws that govern memristor behavior and include information about stochastic properties. Our aim is the introduction of a simple model based on the generalization of the known ones. There are different theoretical models of memristive systems proposed in the literature. They can be ordered in four main approaches: dynamical, microstructural, thermodynamical and stochastic. Below we select only those allowing the description of stochasticity and show that all the stochastic models can be reduced to the same foundations, which can be specified as the model of the overdamped Brownian motion on the field of force.

The dynamical approach is based on rather simple dynamic equations that catch the key physical properties of memristor behavior. The models used in [2, 37–41] and the model of conductive filament (CF) growth in [42] can be attributed to this approach. These models usually involve at least two equations: one is the Ohmic-type relationship between voltage and current and the second is a first-order differential equation for a state variable. The stochasticity is not taken into account by dynamic models, while it appears in the system due to many reasons including uncertainty of the model itself. The uncertainty of the model arises because in the dynamic approach one uses only the basic properties of the memristive system for the model construction and omits some other details. The selected basic properties are mainly defined by the choice of the internal state variable which is not observed from external electrical behavior [40]. There are models of memristive systems described by different state variables such as the doping ratio [40], the width of doping region [39], the concentration of vacancies in the gap region [43], the thickness of CF [42], the tunneling barrier width [44] etc.

The microstructural approach provides more accurate models for all physical processes taking place at the microlevel [45–47]. While the dynamic approach provides a practical fit of an abstract mathematical formulation with generalized experimental data of switching processes, the microstructure models aimed at precisely meeting the physical dynamics of fabricated devices. In this case, the mathematical complexity growths considerably, the model includes a large number of various differential equations and allows only numerical simulation. However, the simulated values sometimes provide only qualitative fit to the experimental data [47]. Indeed, the microstructural model may require dozens of extra physical parameters for simulation and each one can contain some error. As a result, considerable uncertainty in description remains. In addition, due to the increased complexity of this approach, the resulting model does not allow the efficient application of analytical methods for analysis of the system and lead to the long computational procedures.

The thermodynamic models include fluctuations in a natural way. In this approach, the state of a memristive system like in the dynamical approach can be described by an internal state variable, the system parameter, the representative or configurational coordinate, etc. The system tends to the state with the minimal value of a thermodynamic potential, e.g. free energy $\mathcal{F}$ as a function of the internal state variable. According to [48], the free energy of a memristive system may have three local minima separated by

J. Stat. Mech. (2020) 024003

energy barriers. The thermodynamic system can change the locally stable state under the action of fluctuations and due to variation of external parameters (e.g. external electric field). At the equilibrium, the thermodynamic models provide well defined Boltzmann probability distribution of the internal state variable $W(x) = A\exp(-\mathcal{F}(x)/kT)$, where A is a normalization factor. The evolution of nonequilibrium system is often described by the Fokker–Planck equation (FPE) for the probability distribution of the state variable in the field of thermodynamic force, defined by the profile of the free energy [48, 49]. The FPE, which takes fluctuations into account, describes the nonlinear relaxation from the initial nonequilibrium distribution towards that of equilibrium. If there is a constant flow, the system can relax to a nonequilibrium steady state (NESS) [50–52].

In the framework of the stochastic approach, the mathematical models involve the random force. Similar to the dynamic approach the stochastic models are based on at least two equations: an Ohmic-type relationship and a first-order differential equation with a noise source [28, 53, 54]. The stochastic part of the model—the first order Langevin equation—is known as the model of overdamped Browninan motion in the field of force [55]. If, instead of a separate Brownian particle, we consider an ensemble of particles, where each one moves randomly and independently according to the Langevin equation, we can introduce the average concentration of particles per unit space [26, 56, 57]. The appropriate equation for the concentration of particles (or the probability density, if the normalization holds true) is the FPE. Therefore the first order Langevin equation and the FPE are equivalent in the sense they both describe the same dynamics of Brownian particles but with different approaches: the statistical analysis of the random trajectory of the particle or the spatio-temporal behavior of the probability density of the particles [55]. Therefore the thermodynamic and stochastic approaches have a common base and can be considered as variations of the same basic mathematical model.

Thus, the fluctuations are taken into account in an explicit way only in stochastic and thermodynamics models. Though the various stochastic and thermodynamic models are already proposed elsewhere, a deeper investigation of the stochastic behavior of the memristive system is still necessary. It is important to investigate these models not only with numerical simulations, as in complex cases, but also analytically, as in simple but effective cases. As a rule, the exact analytical solutions of simple effective models give rise to deep insight into the physics of the observed phenomena.

Also it is important to study what is the equilibrium, or steady-state, of the memristive system for a set of external parameters, and analyze the related time characteristics such as the relaxation time to the steady-state, the transition time to another equilibrium state and the lifetime of metastable states under the influence of noise. The statistics of switching times and the appropriate probability distributions were investigated in [26, 28, 44, 56–59], and some common properties for the mean switching time values were revealed for different systems investigated. However, these studies, besides their importance, are not sufficient to understand if the main working states of the memristor, that are the high resistance state (HRS) and low resistance state (LRS), appear as equilibrium, nonequilibrium steady, metastable or unstable states. In case they are (or one of them) metastable or unstable, then what is the steady state? Is it an equilibrium state or NESS?

On the other hand, nowadays there are many known examples, where the interplay of nonlinearity and fluctuations can change the properties of a stochastic system in a

J. Stat. Mech. (2020) 024003

counter-intuitive way, in classical and quantum physics [60–72]. Furthermore, internal and external noise can play a positive role in switching dynamics of memristors. In fact, in [53] it was shown that internal noise helps to increase the contrast ratio between low and high resistance states, and in [73] the authors experimentally observed, in a memristor system, a phenomenon similar to stochastic resonance [74–76] with a beneficial role of noise in resistive switching. In particular, they studied the effect of external noise on the resistive switching of a memristor system and found an optimal noise amplitude that maximizes the contrast between HRS and LRS. However, basic stochastic properties, such as the stationary and non-stationary distribution of diffusing particles in memristors, the relaxation or the transition time, have not been investigated.

In this paper, we introduce a stochastic model of a memristor, based on a generalization of known approaches and experimental results. By solving numerically the FPE under periodic voltage driving we get the $I - V$ characteristic for our theoretical model in one-dimensional case. We validate our theoretical $I - V$ characteristic by an experiment reported here with a newly engineered memristive device based on the $Au/Ta/ZrO_2(Y)/Ta_2O_5/TiN/Ti$ multilayer structure and by experiments shown in [77] and references therein. The agreement between the theoretical and experimental $I - V$ characteristics is quite good and shows that the model is able to reproduce the main fundamental properties of memristive system: the hysteresis of $I - V$ characteristic and its dependence on the frequency of the driving signal. Our theoretical approach is similar to that proposed in [26, 54, 56, 59]. However, we study our model not only numerically but also analytically, obtaining the exact analytical expressions for non-equilibrium distributions in the one-dimensional case, for two types of boundary conditions. The exact analytical solutions obtained are an effective tool to analyze the transient dynamics of the memristors and at the same time provide a way to improve the theoretical techniques to investigate the memristor devices in a vast area of parameters and conditions. We analyze the influence of fluctuations and other parameters on the relaxation time to the steady-states. We find that the relaxation time shows a non-monotonic dependence on the intensity of the fluctuations. For particular forms of potential profiles, that describe the structure of the dielectric material, the relaxation time can be reduced.

2. Description of the generalized stochastic model

The main physical parameter describing the state of a memristor is its resistance. Among a wide variety of resistive-switching memory devices implemented with different materials, a significant part is based on the formation and destruction of the CF in a thin dielectric film by applying an external voltage. The stochasticity of the memristors is manly attributed to this process [6, 24, 28]. The process of CF formation and destruction is based on a random hopping of the metal ions or dielectric structural defects (oxygen vacancies), which are positively charged, between the trapping sites within the structure of dielectric material. Let us call these ions or vacancies as diffusing particles. This diffusion process leads eventually to the formation or destruction of CF,

J. Stat. Mech. (2020) 024003

depending on the direction of the external electric field, which defines the average drift direction. A conducting path is thus formed through the areas where the concentration of the particles is high enough. Following [54] we describe the motion of these particles by a Langevin equation

$$\eta \frac{\mathrm{d}x}{\mathrm{d}t} = -\frac{\partial U(x,V)}{\partial x} + \xi(t), \tag{1}$$

where x is the coordinate of a particle, η is the coefficient of viscosity, $U(x,V)$ is the potential profile defining the regular force acting on the particles which depends on the voltage V of the electrodes of the memristor, and $\xi(t)$ is a white Gaussian noise with the usual statistical properties $\langle\xi(t)\rangle = 0$ and $\langle\xi(t)\xi(t+\tau\rangle = 2\theta\delta(\tau)$, where $\delta(\tau)$ is the delta function and 2θ is the noise intensity. When the fluctuations have only thermal nature, the intensity is proportional to the temperature $\theta = \eta k_{\mathrm{B}}T$, where T is the temeperature and k_{B} is the Boltzmann constant, according to the Sutherland–Einstein relation. The average concentration of randomly walking particles as a function of time and space coordinate is used as internal state parameter defining the state of the memristor. Following [56, 57, 59], for simplicity of analysis, we consider the one-dimensional model, which can be generalized to three-dimensional if necessary. Let the top electrode (TE) be positioned at $x = 0$ and the bottom electrode (BE) at $x = L$. The uncertainty provided by the model itself and the inevitable uncertainties in the calculation of macrophysical parameters (such as electrical and thermal conductivity of the material, viscosity, variations in activation energies for defect and electron transport, etc), inaccurate control of the structure and boundary conditions, imprecise control of the initial conditions (such as the initial concentration of the defects, the inhomogeneity of the initial states, etc) and the presence of thermal fluctuations are described by the stochastic force $\xi(t)$ (see equation (1)), whose intensity is proportional to the temperature in the presence of only thermal fluctuations.

The potential profile $U(x,V)$ for hopping particles is represented by the potential wells separated by the barriers (see figure 1). The height of the barriers is the activation energy E_a, which must be provided to the hopping particle to surmount the barrier and move to the neighboring well in a random direction. Besides the periodic component $\Phi(x)$ of the function $U(x)$, the external field provides the slope F of the potential profile directed to one or another electrode depending on the polarity of the applied voltage as it is shown in figures 1(a)–(c)

$$U(x,V) = \Phi(x) - Fx, \tag{2}$$

where $F = qV/\varepsilon L$, q is the charge of the particle and ϵ is the dielectric constant.

Special conditions for the potential appear near the electrodes. Using various electrode materials, we can modify the energy properties of the interface that influence the shape of the potential profile near the boundaries at $x = 0$ and $x = L$. The role of these changes can be important as it can influence the resistance values in LRS and HRS as well as the properties of the switching dynamics [78, 79]. Usually, TE has a low and easily oxidizable work function (WF) and BE has a higher WF. In general, it can be taken into consideration by an additional potential well with the depth E_t near the TE and the potential barrier with the height E_b near BE, as shown in the figures 1(d)–(f). In this paper we consider only two special cases, when $E_t = E_b = E_a$ and when $E_b \to \infty$ under $E_t = E_a$. The latter case corresponds to a BE consisting of an ideally inert material.

J. Stat. Mech. (2020) 024003

The Langevin equation (1) corresponds to the following Fokker–Planck equation (FPE) for the concentration of particles $n(x,t)$

$$\frac{\partial n}{\partial t} = \frac{1}{\eta}\frac{\partial}{\partial x}\left[\frac{\partial U(x,V)}{\partial x}n\right] + D\frac{\partial^2 n}{\partial x^2}, \tag{3}$$

where $D = \theta/\eta^2$ is the diffusion coefficient. Further in the paper, we will consider $\eta = 1$. The Brownian diffusion in tilted periodic potential (2), described by equation (3), can be replaced by the diffusion in the flat tilted potential U_1 without barriers [55, 80–84, 86]

$$U_1(x,V) = -v_{\mathrm{eff}}x, \tag{4}$$

with the effective drift and diffusion coefficients v_{eff} and D_{eff}, respectively. As a result, equation (3) for the coarse-grained concentration of particles $n_1(x,t)$ takes the following form

$$\frac{\partial}{\partial t}n_1(x,t) = \frac{\partial}{\partial x}\left[n_1(x,t)\frac{\partial U_1(x,V)}{\partial x}\right] + D_{\mathrm{eff}}\frac{\partial^2}{\partial x^2}n_1(x,t) \tag{5}$$

and the exact expressions for the effective drift and diffusion coefficients, valid for arbitrary values of $F = qV/\varepsilon L$ and θ, are the following [82, 83]

$$v_{\mathrm{eff}} = \frac{\ell}{T_1(x_0, x_0+\ell)}, \tag{6}$$

$$D_{\mathrm{eff}} = \frac{\ell^2}{2}\frac{\Delta T_2(x_0, x_0+\ell)}{[T_1(x_0, x_0+\ell)]^3}, \tag{7}$$

where ℓ is the period of the periodic component $\Phi(x)$ of the potential (2), T_1 is the mean first passage time (FPT) of the particle through the boundary $x_0+\ell$, when it starts from the point x_0, and ΔT_2 is the variance of this FPT. If for any value of external voltage V we can consider that the resulting energy of activation is much greater than the intensity of fluctuations, $E \approx E_a - F\ell/2 \gg \theta$, then we can use the following approximate expressions for (6) and (7)

$$v_{\mathrm{eff}} = \frac{2\ell}{\tau_{kr}}\sinh\frac{F\ell}{2\theta}, \tag{8}$$

$$D_{\mathrm{eff}} = \frac{\ell^2}{\tau_{kr}}\cosh\frac{F\ell}{2\theta}, \tag{9}$$

where τ_{kr} is the Kramers time

$$\tau_{kr} = \tau_0 \exp\frac{E_a}{\theta}. \tag{10}$$

Here E_a is the activation energy for zero bias and $\tau_0(\theta)$ is defined by the specific shape of the periodic potential $\Phi(x)$. For thermal fluctuations, $\theta = k_{\mathrm{B}}T$, the expressions (8) and (9) satisfy the following relation [87]

$$D_{\mathrm{eff}} = \theta\frac{d}{dF}v_{\mathrm{eff}}. \tag{11}$$

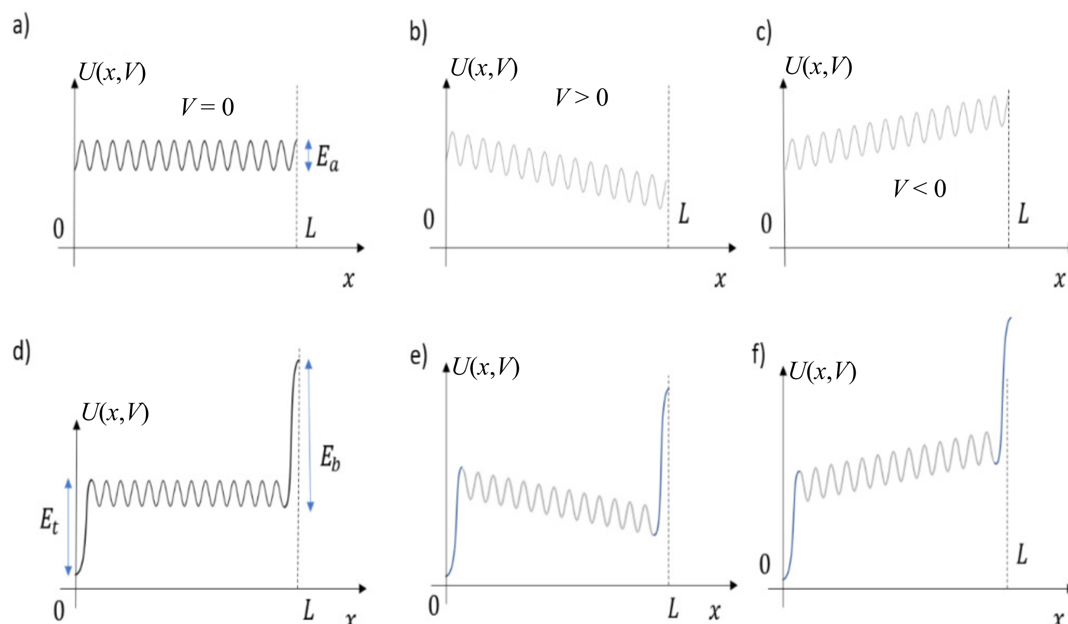

Figure 1. View of the potential profile $U(x, V)$ defining the regular force acting on diffusing particles under zero external bias $V = 0$ ((a), (d)), positive $V > 0$ corresponding to ON set ((b), (e)) and negative $V < 0$ corresponding to OFF set ((c), (f)). The view of potential profile taking into account the influence of the TE and BE materials (d)–(f) in a general case.

The approximate expressions for effective drift and diffusion coefficients (8) and (9) provide a monotonic dependence on the parameters θ and F and were obtained under some specific assumption about the shape of the periodic potential profile $\Phi(x)$. Namely, the width of the barriers is about the width of the wells and the top of each barrier is in the middle between two nearby wells for any value of F. The real shape of the potential profile is defined by the specific structure of the dielectric material and can be different. It was shown in [82–85] that the functions $D_{\text{eff}}(\theta)$ and $D_{\text{eff}}(F)$ can be nonmonotonic for some particular shapes of potential wells and barriers. For example, these functions will have a maximum if the potential profile $\Phi(x)$ has wide wells and narrow barriers or vice versa, as it is shown in the inset (a) and (b) of figure 2. A similar potential profile can be created by inserting rows of metallic nanoparticles into the dielectric layer [88]. This nonmonotonicity with a maximum is a signature of the phenomenon of acceleration of diffusion in subcritically tilted periodic potentials [82, 84, 85]. To take it into account, we should use the exact expressions for the effective drift and diffusion coefficients (6) and (7).

The complete memristor model, in addition to the drift-diffusion equation (5) and Ohmic type relationship, should also include the equations that connect the coarse-grained concentration of the defects $n_1(x,t)$ with the resistance R, taking into account that the current I flowing between the electrodes heats the material locally and therefore contributes to the increase of the noise intensity. It can also be taken into account that the electric field inside the memristor can be distorted since there are areas with different conductivity depending on the $n_1(x,t)$ distribution. Therefore, in a general case one can consider the potential field as a function of a greater number of parameters

J. Stat. Mech. (2020) 024003

$U_1(x, V, I, n_1)$ obeying the additional equations and then the FPE (5) can become nonlinear in n_1. Note that the drift term in equation (5) can be represented as the following sum

$$\frac{\partial}{\partial x}\left[\frac{\partial U_1(x,V,I,n_1)}{\partial x}n_1\right] = \frac{\partial U_1(x,V,I,n_1)}{\partial x}\frac{\partial n_1}{\partial x} + \frac{\partial^2 U_1(x,V,I,n_1)}{\partial x^2}n_1. \tag{12}$$

The influence of Joule heating was investigated numerically in [26, 45–47] for the three-dimensional case. The case $U_1 = U_1(x, n_1)$ was investigated in [56] for one-dimensional case with the assumption that the second term in (12) can be neglected. This is true when $U_1(x)$ is a linear function. The Joule heating effect was not considered in [56]. In the present paper we consider the most simple case, when Joule heating and nonlinear effects are not taken into account. The specific form of $R(n_1)$ is not crucial for the model considered here and depends on the properties of specific materials. Further we consider the case when a low value of n_1 leads to high resistance and vice versa [89]. Let this dependence be strongly nonlinear and threshold-like: the resistance is drastically reduced when n_1 becomes greater than a threshold value $n_1 = n_{\mathrm{th}}$. In this simplified case, the total resistance of the memristor can be calculated as follows [2]

$$R_m = R_{\mathrm{ON}}\frac{w(t)}{L} + R_{\mathrm{OFF}}\left(1 - \frac{w(t)}{L}\right), \tag{13}$$

where $w(t)$ is the size of the doped region, R_m is the memristor resistance and R_{ON} is the low value of the resistance, when the concentration of defects exceeds the threshold level $n_1(x, t) > n_{\mathrm{th}}$ and R_{OFF} is the high value of resistance, when $n_1(x, t) < n_{\mathrm{th}}$ (see figure 3).

Note that equation (5) is the same drift-diffusion equation that describes the movement of particles in a memristive system mentioned in [59], in which its one-dimensional solution is investigated. In [26], we can find the three-dimensional version of this equation which is solved only numerically. In [56] equation (5) is considered nonlinear, when $U_1(x, V) = U_1(x, V, n_1)$, but the second term in the expansion (12) is neglected. In this case FPE (5) is treated as a generalized Burgers' equation. In the next section, we compare the $I - V$ characteristic obtained in the proposed simple one-dimensional linear model with the experimental one.

3. Comparison with experiment

To validate the stochastic model of a memristive device described in the previous section, we verify the fundamental properties of resistive switching such as the $I - V$ characteristic and its dependence on the driving frequency. The experimental memristive device used for validation was fabricated on the basis of a newly engineered $Au/Ta/ZrO_2(Y)/Ta_2O_5/TiN/Ti$ multilayer structure, which is described in more details in [90]. $I - V$ sweep measurements were carried out at room temperature in atmospheric conditions by using the Agilent B1500A semiconductor device analyzer. The measured $I - V$ characteristics are presented in figure 4 by color lines, where the colors correspond to the different cycles.

J. Stat. Mech. (2020) 024003

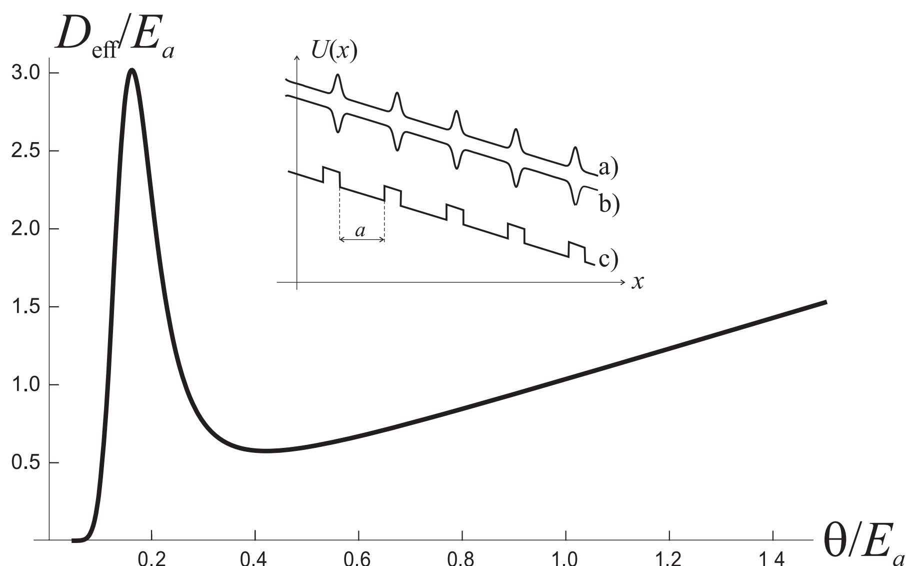

Figure 2. Effective diffusion coefficient as a function of dimensionless fluctuation intensity θ/E_a for potential profile (c) shown in the inset with the value $a = 0.8\ell$. Inset: examples of tilted periodic potentials for which the acceleration of diffusion can be observed. E_a is the activation energy or the barrier height at $V = 0$.

The sweeping period is 4s and sweeping amplitude is 3 V. The sign of bias on the device corresponds to the potential of the Au electrode relative to the grounded TiN/Ti electrode. The experimental memristive device demonstrates typical bipolar switching of anionic type related to reconstruction and destruction of the CF composed of oxygen vacancies [91]. The SET process at positive bias corresponds to the transition from HRS to LRS. The backward transition at negative bias is denoted as the RESET process in figure 4.

The results of numerical solution of equations (4), (5), (8)–(10) and (13) are shown by the black line in figure 4. For the model test we use the following parameters: the dimensionless activation energy in the equations (8)–(10) is $E_a/\theta = 23$, which becomes $E_a = 0.6\,\text{eV}$ at room temperature, when fluctuations have the thermal nature $\theta = k_\text{B}T$. This is in agreement with recent measurements of activation energy based on the analysis of flicker noise generated by a memristive device [92]. The maximum dimensionless variation of activation energy corresponding to the maximal value of the sweeping voltage $V = 2.2$ V is $\Delta E/\theta = 4.23$. The other parameter values are $\ell^2/\tau_0 = 6 \cdot 10^{-13}$ cm^2 s^{-1} and $L = 10\,\text{nm}$ (the length of the structure). The sweeping period is 4s and the sweeping amplitute 2.2 V. For modeling we used the following boundary conditions

$$n_1(0,t) = N_1,\; n_1(L,t) = N_2, \tag{14}$$

where 0 and L are the coordinates of the TE and BE made of different materials. For the relative concentration of defects at the boundaries, we consider $N_1 = 100\%$ for the easily oxidizable TiN/Ti electrode and $N_2 = 25\%$ for the opposite electrode, which assumes that its ability to provide defects is 4 times lower. Such an assumption may be appropriate for a BE consisting of non-ideal inert material. In the case of an ideal inert material we should use at the BE the reflective boundary conditions, which could

J. Stat. Mech. (2020) 024003

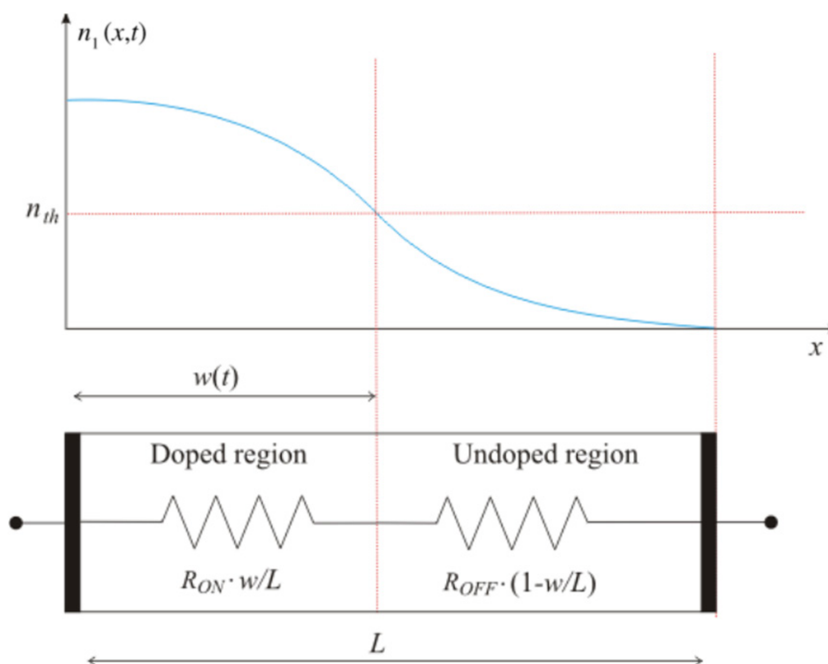

Figure 3. Diagram with the equivalent electric circuit of the memristor model.

be more appropriate for Au in the case of high material purity. The threshold value of the concentration for resistance switching is $n_{\text{th}} = 50\%$.

Comparing the experimental and simulated results shown in the figure 4 we can see that our theoretical model describes the experiment with a quite good qualitatively agreement and captures the key fundamental properties of the real $I - V$ characteristic. There is a hysteresis on the characteristic $I - V$ and its area and shape correspond to that observed in the experiment. During the SET process, the sharp switching from HRS to LRS appears at approximately the same voltage, that is around 2 V. The SET value of the current is different because the current through the experimental sample is limited by the compliance current $I_c = 300\ \mu$A. The equations introduced in section 2 do not model the circuits for current restriction at the SET regime. Therefore the value of the resistance in LRS reached in the model is less comparable to that in the experiment. Additional conditions that model the limitation of the current can be added to our model, if necessary, while it is not crucial for the model verification.

In the RESET regime we can see that the switching process from LRS to HRS starts approximately at the same value of driving voltage $V = -1.1$ V, but the model switches to the HRS state slightly faster. This difference may be due to the particular choice of boundary conditions. The conditions (14), used for the test of the model, allow to reduce the concentration of defects at $V < 0$ by two ways: by inverse flow of the defects back to the TE located at $x = 0$ and through the BE boundary at $x = L$, which works as the sink of defects, when $n_1(L, t) > N_2$. If we consider the reflecting boundary condition at $x = L$, suitable for an ideally inert material of the electrode, the dispersion of the defects through the electrode will become impossible and we will observe a slowing down of the switching process. On the other hand, in the literature we can find the experimental data with $I - V$ characteristics that show a faster RESET process

J. Stat. Mech. (2020) 024003

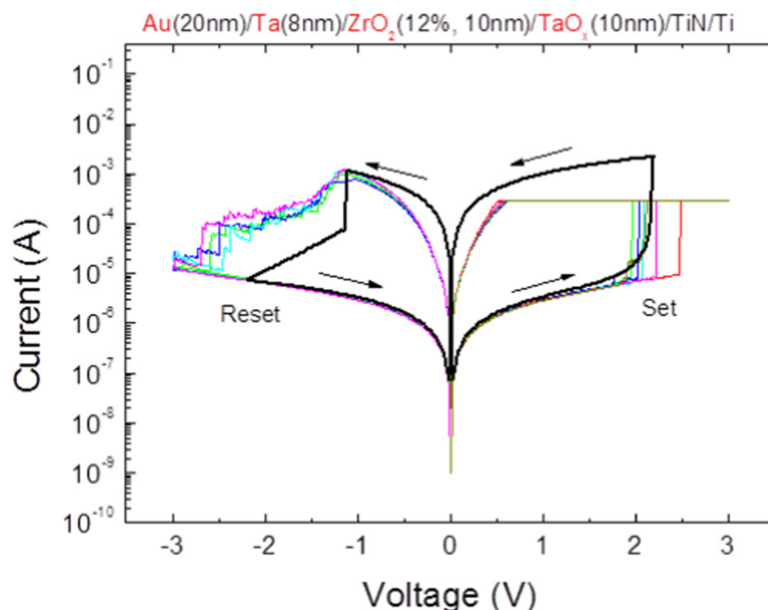

Figure 4. $I-V$ characteristic of the memristive device. Color lines: experimental, measured on the device based on $Au/Ta/ZrO_2(Y)/Ta_2O_5/TiN/Ti$ structure (different colors correspond to different switching cycles). Black line: theoretical, based on numerical solution of equations (4), (5), (8)–(10) and (13) with boundary conditions (14). Voltage sweeping period is 4s. Other parameters used for numerical solution: $E_a/\theta = 23$, $\Delta E/\theta = 4.23$, $\ell^2/\tau_0 = 6\cdot 10^{-13}$ cm^2 s^{-1}, $L = 10$ nm, $N_1 = 100\%$, $N_2 = 25\%$, and $n_{\rm th} = 50\%$.

appropriate to the result of the above simulation with boundary conditions (14) (see, for example, [93]).

The precise modeling of particular experimental processes is not the main topic of this paper. Our aim is to demonstrate that our simple model is able to reproduce the main features of real memristive devices. Another fundamental property is the shrinking of the hysteresis loop with increasing driving frequency [77]. This basic property is captured by the proposed model, as we can see from figure 5, where the theoretical $I-V$ characteristic, with the same parameters but for different values of driving frequencies, is shown. This dependence of hysteresis of the $I-V$ characteristic on the driving frequency is in agreement with experimental results shown in [77] and references therein. A more detailed fitting of the proposed model to specific experiments is the subject of forthcoming work.

In the next section, we show that the proposed model is not only able to capture the key properties of real memristive systems, but allows us to obtain the exact analytical solutions, which implies the qualitative and quantitative improvement of the theoretical techniques to analyze such systems in different physical conditions.

4. Exact solution and analysis

The stationary solution $n_{\rm st}(x)$ of the FPE (5) obeys the following equation

J. Stat. Mech. (2020) 024003

$$\left[\frac{\partial}{\partial x}\frac{\partial U_1(x,V)}{\partial x} + D_{\text{eff}}\frac{\partial^2}{\partial x^2}\right] n_{\text{st}}(x) = 0. \tag{15}$$

For the linear potential profile (2) the equation (15) reads

$$D_{\text{eff}}\frac{\mathrm{d}^2 n_{\text{st}}(x)}{\mathrm{d}x^2} - v_{\text{eff}}\frac{\mathrm{d}n_{\text{st}}(x)}{\mathrm{d}x} = 0. \tag{16}$$

Taking the boundary conditions (14) one may obtain the following stationary solution (shown in figure 6(a))

$$n_{\text{st}}(x) = \frac{N_2 - N_1}{\exp\left(\frac{v_{\text{eff}}L}{D_{\text{eff}}}\right) - 1}\left[\exp\left(\frac{v_{\text{eff}}x}{D_{\text{eff}}}\right) - 1\right] + N_1. \tag{17}$$

As we mentioned before, if the BE is made of inert material with a very high WF, it can be modeled as a reflecting boundary, that is an infinitely high barrier, for the defects at the point $x = L$. Replacing boundary conditions (14) with the following ones (18)

$$n_{\text{st}}(0) = N_1,\; G_{\text{st}}(L) = v_{\text{eff}} n_{\text{st}}(L) - D_{\text{eff}}\frac{\mathrm{d}n_{\text{st}}(x)}{\mathrm{d}x}\bigg|_{x=L} = 0, \tag{18}$$

where $G_{\text{st}}(L)$ is the stationary flux of the diffusing defects at the point $x = L$, we can repeat the whole procedure and obtain the following equilibrium concentration which is shown in figure 6(b)

$$n_{\text{st}}(x) = N_1 \exp\left(\frac{v_{\text{eff}}x}{D_{\text{eff}}}\right). \tag{19}$$

We can see that for reflecting boundary conditions (18), the variations of $n_{\text{st}}(L)$ with external bias F is much wider than that obtained with the boundary conditions (14). This means that the amplitude of the resistive switching between LRS and HRS will be greater when the BE material is inert. The same conclusion was realized in [78] based on experimental results. An exponential dependence of the resistance value from the maximum reset voltage has been experimentally observed also in memristive devices with inert BE [79]. The concentration (19) corresponds to the equilibrium state of the system described by (5), while the concentration (17) appears in the NESS because there is the constant flow of defects between the electrodes in this steady state.

Now we can find the nonstationary solution of equation (5). This allows us to see how the concentration of defects evolves with time as one changes external voltage, noise intensity, effective diffusion coefficient and other parameters, such as the temperature. As a consequence, the relaxation processes can speed up or delay. Let us consider first the boundary conditions (14) and write the general solution $n_1(x,t)$ of equation (5) as a sum of two terms

$$n_1(x,t) = n_{\text{st}}(x) + n_{\text{nst}}(x,t), \tag{20}$$

where $n_{\text{st}}(x)$ is the stationary part (17) satisfying the boundary conditions (14) and $n_{\text{nst}}(x,t)$ is the nonstationary part with zero boundary conditions

$$n_{\text{nst}}(0,t) = n_{\text{nst}}(L,t) = 0.$$

J. Stat. Mech. (2020) 024003

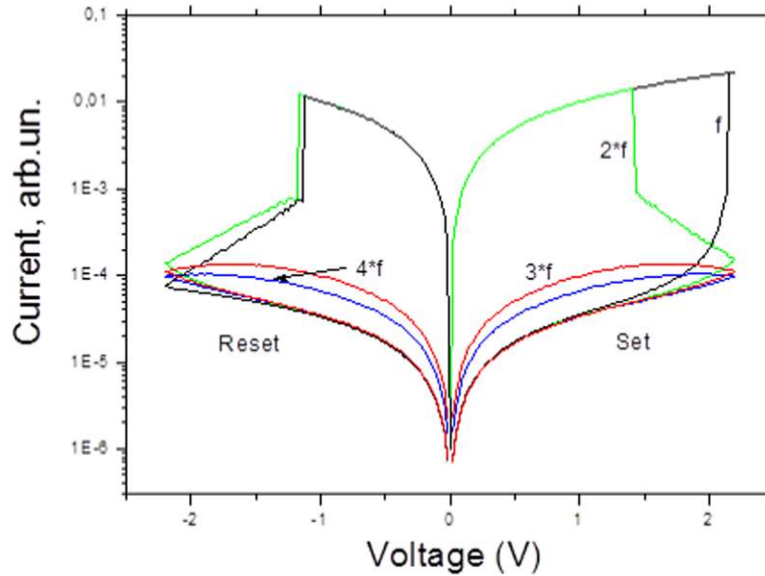

Figure 5. Theoretical $I-V$ characteristic for different driving frequencies: black is for $f=0.25$ Hz, the same frequency as for the black plot in figure 4, Green—$2f$, Red—$3f$, and Blue—$4f$. The other parametrs of the model are equal to those used for figure 4.

Taking the non-stationary part as a function with separable variables

$$n_{\rm nst}(x,t)=T(t)S(x), \tag{21}$$

we transform equation (5) into the following form

$$S(x)\frac{{\rm d}T(t)}{{\rm d}t}=-T(t)v_{\rm eff}\frac{{\rm d}S(x)}{{\rm d}x}+T(t)D_{\rm eff}\frac{{\rm d}^2S(x)}{{\rm d}x^2}. \tag{22}$$

Now, by grouping terms with spatial and temporal variables, we finally obtain the equations for the functions $S(x)$ and $T(t)$

$$\frac{{\rm d}T(t)}{{\rm d}t}=CT(t), \tag{23}$$

$$\frac{{\rm d}^2S(x)}{{\rm d}x^2}-\frac{v_{\rm eff}}{D_{\rm eff}}\frac{{\rm d}S(x)}{{\rm d}x}-\frac{C}{D_{\rm eff}}S(x)=0, \tag{24}$$

where C is an arbitrary constant, which should be negative or equal to zero to make solution (23) bounded

$$T(t)=C_1{\rm e}^{Ct}. \tag{25}$$

Linear and homogeneous equation (24) has two characteristic roots $\lambda_{1,2}$

$$\lambda_{1,2}=\frac{1}{2}\left(\frac{v_{\rm eff}}{D_{\rm eff}}\pm\sqrt{\left(\frac{v_{\rm eff}}{D_{\rm eff}}\right)^2+4\frac{C}{D_{\rm eff}}}\right). \tag{26}$$

Since the constant C is negative or equal to zero, the characteristic roots $\lambda_{1,2}$ may be either real or complex. For the real ones, the solutions of the equation (24) are

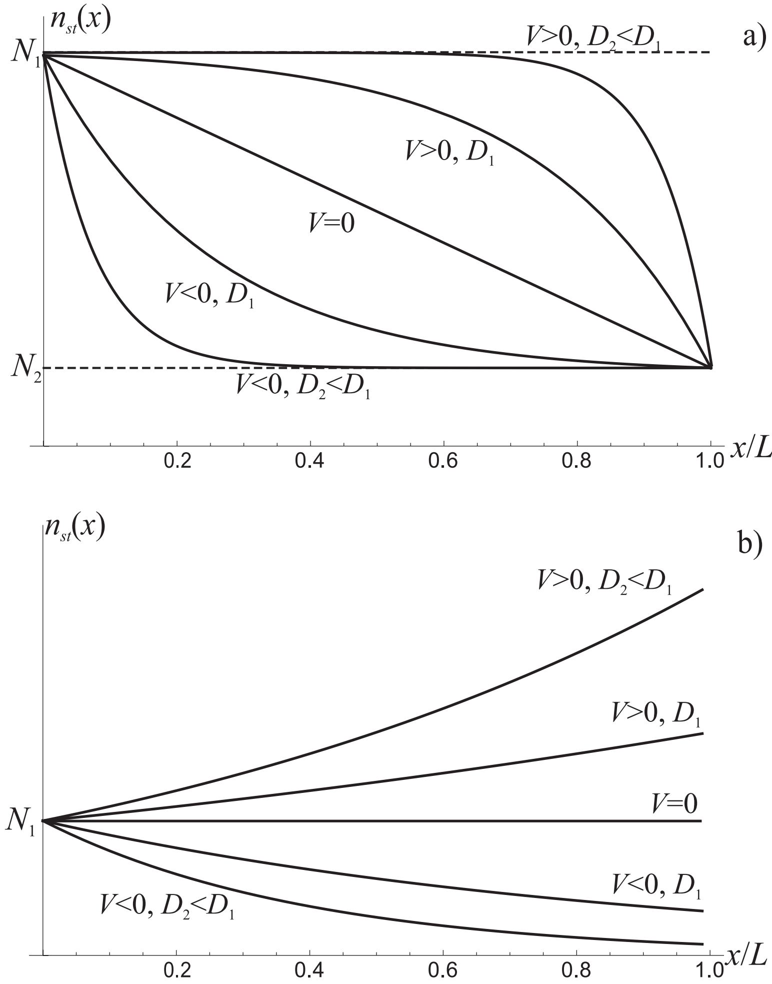

Figure 6. Steady-state concentration $n_{\mathrm{st}}(x)$ for different values of bias V and diffusion coefficient D_{eff} equal to two different values D_1 and D_2 such that $D_2 < D_1$: (a) for boundary conditions (14); (b) for boundary conditions (18) corresponding to the ideally inert material of the BE.

$$S(x) = C_2 \exp\left[\frac{x}{2}\left(\frac{v_{\mathrm{eff}}}{D_{\mathrm{eff}}} + \sqrt{\left(\frac{v_{\mathrm{eff}}}{D_{\mathrm{eff}}}\right)^2 + \frac{4C}{D_{\mathrm{eff}}}}\right)\right] + C_3 \exp\left[\frac{x}{2}\left(\frac{v_{\mathrm{eff}}}{D_{\mathrm{eff}}} - \sqrt{\left(\frac{v_{\mathrm{eff}}}{D_{\mathrm{eff}}}\right)^2 + \frac{4C}{D_{\mathrm{eff}}}}\right)\right], C < 0 \tag{27}$$

$$S(x) = C_4 + C_5 \exp\left(\frac{v_{\mathrm{eff}} x}{D_{\mathrm{eff}}}\right), C = 0.$$

However, in this case, according to the boundary conditions $S(0) = S(L) = 0$ all arbitrary constants C_2, C_3, C_4, C_5, are equal to zero. Thus, the constant C should be chosen in such a way that the characteristic roots $\lambda_{1,2}$ are complex

$$\lambda_{1,2} = a \pm ib, \tag{28}$$

J. Stat. Mech. (2020) 024003

where

$$a = \frac{v_{\mathrm{eff}}}{2D_{\mathrm{eff}}}, \tag{29}$$

$$b = \frac{1}{2}\sqrt{-\left(\frac{v_{\mathrm{eff}}}{D_{\mathrm{eff}}}\right)^2 - 4\frac{C}{D_{\mathrm{eff}}}}, \tag{30}$$

and, because the solution $S(x)$ should be real, we consider the constraint $C_3 = C_2^*$ for the complex coefficients C_2 and C_3 of equation (27). With this choice of the constants C, C_2, C_3, we obtain the following solution of the equation (24)

$$S(x) = \mathrm{e}^{ax}\left[\hat{C}_2 \sin(bx) + \hat{C}_3 \cos(bx)\right], \tag{31}$$

where $\hat{C}_2$ and $\hat{C}_3$ are new real unkown constants. Finally, using boundary conditions

$$S(0) = \hat{C}_3 = 0,\ S(L) = \hat{C}_2 \sin(bL) = 0, \tag{32}$$

one can find the equation for the constant C

$$\frac{L}{2}\sqrt{-\left(\frac{v_{\mathrm{eff}}}{D_{\mathrm{eff}}}\right)^2 - 4\frac{C}{D_{\mathrm{eff}}}} = \pi n. \tag{33}$$

Therefore, the set of possible values of the constant C is the following

$$C(n) = \frac{D_{\mathrm{eff}}}{4}\left(-\frac{4(\pi n)^2}{L^2} - \left(\frac{v_{\mathrm{eff}}}{D_{\mathrm{eff}}}\right)^2\right) < 0,\ n = 0, 1, 2, \ldots \tag{34}$$

As a result, according to equations (23) and (31) the nonstationary solution may be written as follows

$$n_{\mathrm{nst}}(x,t) = \sum_{n=0}^{\infty} C_1(n)\mathrm{e}^{C(n)t}\mathrm{e}^{ax}\hat{C}_2(n)\sin\left(\frac{\pi n x}{L}\right). \tag{35}$$

Denoting the product of $C_1(n)$ and $\hat{C}_2(n)$ as a new constant $C_0(n)$, we finally obtain

$$n_{\mathrm{nst}}(x,t) = \exp\left(\frac{v_{\mathrm{eff}}x}{2D_{\mathrm{eff}}}\right)\sum_{n=0}^{\infty} C_0(n)\exp\left[C(n)t\right]\sin\left(\frac{\pi n x}{L}\right), \tag{36}$$

where the set of arbitrary constants $C_0(n)$ is defined by the initial conditions

$$C_0(n) = \frac{2}{L}\int_0^L \exp\left(-\frac{v_{\mathrm{eff}}x}{2D_{\mathrm{eff}}}\right) n_{\mathrm{nst}}(x,0)\sin\left(\frac{\pi n x}{L}\right)\mathrm{d}x. \tag{37}$$

Equations (36)–(37) are the exact nonstationary solution of FPE (5) with the boundary conditions (14). Figure 7(a) shows the nonstationary concentration of the defects $n_1(x,t)$ for different times during the set process under $V > 0$ and constant, when the system is switched from HRS to LRS. The area of the doped region, initially located only close to TE, it grows and reaches steady state, in which the doped region fills almost all the area from TE to BE. According to equation (13) it corresponds to the

J. Stat. Mech. (2020) 024003

switching of the resistance value from HRS to LRS. The growth process of the doped region is qualitatively similar to the drift-diffusion model introduced in [59], but in our case we do not need to introduce any additional constrains in the equations of the model, the so-called window functions (see also [39–41]). The nonstationary concentration (36) naturally evolves towards the stationary one under the action of regular and random forces.

The nonstationary concentration $n_1(x,t)$ for the reflecting boundary conditions (18) can be obtained with the same theoretical procedure starting from equation (20), with the first term given by equation (19). Similarly to the equation (36) the nonstationary term reads

$$n_{\mathrm{nst}}(x,t) = \exp\left(\frac{v_{\mathrm{eff}}x}{D_{\mathrm{eff}}}\right)\sum_{n=0}^{\infty} C_0(n)\exp\left(C(n)t\right)\sin b(n)x \tag{38}$$

with differences only in the equations for the constants C, a and b. From the boundary conditions (18) it follows

$$S(0) = 0, \tag{39}$$

$$v_{\mathrm{eff}}S(L) - D_{\mathrm{eff}}\frac{\mathrm{d}S(x)}{\mathrm{d}x}\bigg|_{x=L} = 0. \tag{40}$$

Consequently, instead of equation (32) we get

$$\hat{C}_3(n) = 0, \tag{41}$$

$$\hat{C}_2(n)\left[\left(\frac{v_{\mathrm{eff}}}{D_{\mathrm{eff}}} - a\right)\sin(bL) - b\cos(bL)\right] = 0. \tag{42}$$

Taking into account equations (29) and (30), the expression (42) leads to the following transcendental equation for a and b

$$\tan(bL) = \frac{b}{a}, \tag{43}$$

which has no analytic solution but can be solved numerically or graphically. The plot of nonstationary concentration of particles $n_1(x,t)$ for reflecting boundary (18) is shown in figure 7(b) for different times during the set process under $V > 0$, when the system is switched from HRS to LRS.

For the understanding of switching variability of resistance values in LRS and HRS it is important to compare the switching time observed in experiment with the relaxation time of the defects concentration towards the stationary state. In other words, for the complete analysis it is necessary to understand if the system under observation has reached the stationary state or it remains far from equilibrium. Now, the information about the relaxation time τ towards the steady-state concentration, under the boundary conditions (14), can be easily extracted from equation (34). Indeed, for every space coordinate x the function $n_{\mathrm{nst}}(x,t)$ tends to zero with time as a sum of exponentials. The slowest one of them corresponds to the rate $C(1)$

J. Stat. Mech. (2020) 024003

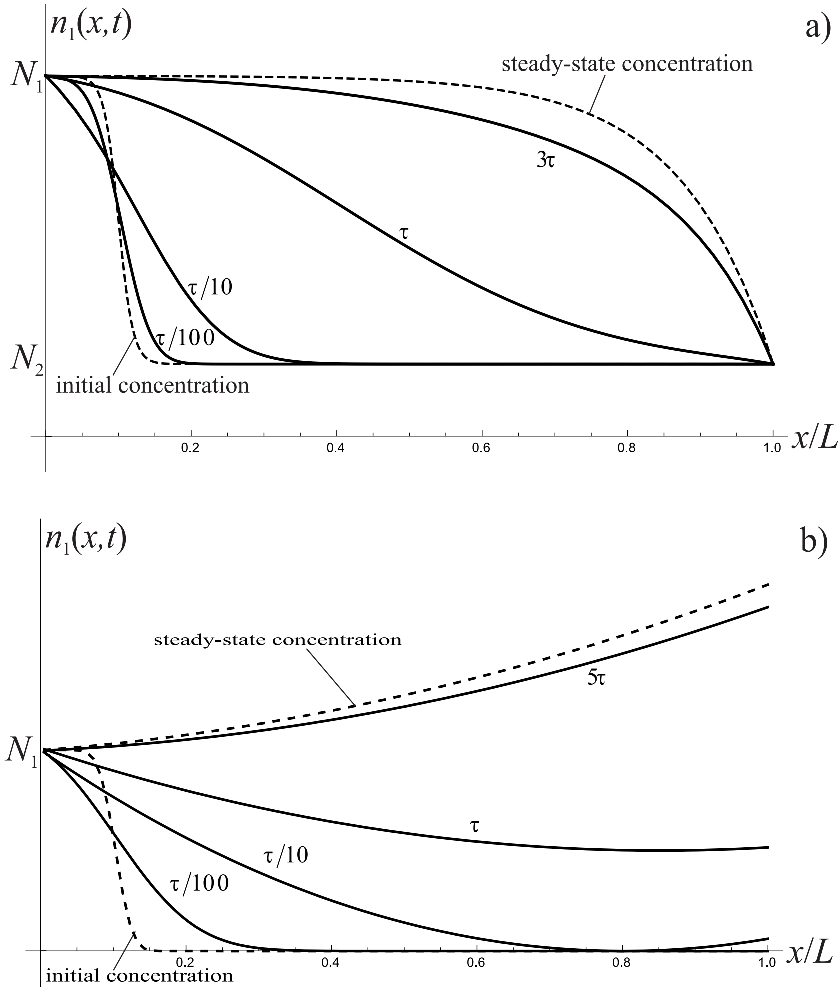

Figure 7. Evolution of nonstationary concentrations (36) and (38) from initial state to the steady-state ON under $V > 0$ and constant, for times multiple of relaxation time τ: (a) for boundary conditions (14); (b) for boundary conditions (18) corresponding to the ideally inert material of the BE.

$$C(1) = -\frac{D_{\text{eff}}}{4}\left(\frac{4\pi^2}{L^2} + \left(\frac{v_{\text{eff}}}{D_{\text{eff}}}\right)^2\right). \tag{44}$$

Thus, the relaxation time reads

$$\tau = \frac{-1}{C(1)} = \left(\frac{2L}{v_{\text{eff}}}\right)\frac{2D_{\text{eff}}/v_{\text{eff}}L}{1+\pi^2\left(2D_{\text{eff}}/v_{\text{eff}}L\right)^2}. \tag{45}$$

The relaxation time (45) as a function of the bias voltage is shown in figure 8 for two values of fluctuation intensity. In accordance with known theoretical and experimental results [28, 58, 59], this dependence is close to the Arrhenius law, which is shown by dashed lines in figure 8. The exact expression $\tau(V)$ deviates from the Arrhenius law for small voltages, when the switching times become large.

J. Stat. Mech. (2020) 024003

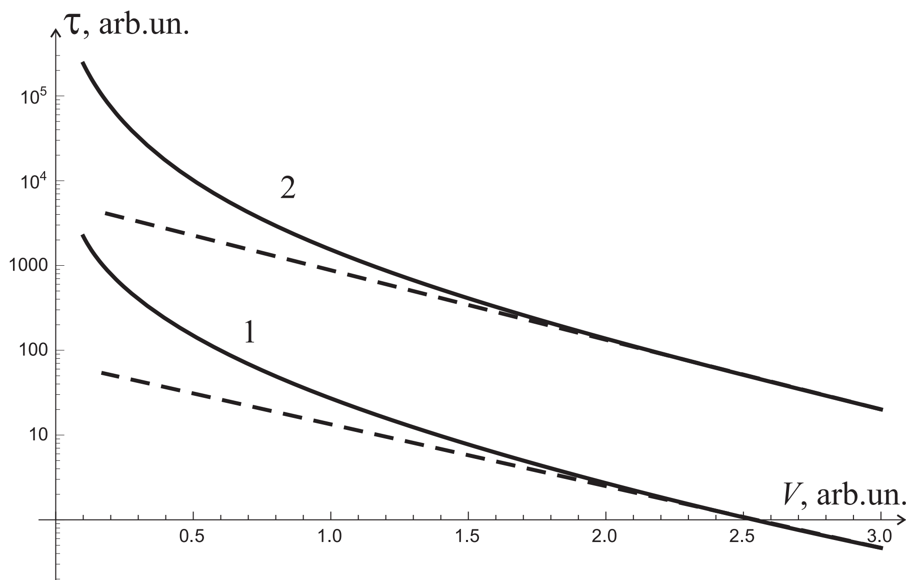

Figure 8. Relaxation time as a function of bias voltage for two values of noise intensity θ_1 (curve 1) and θ_2 (curve 2), with $\theta_1 > \theta_2$. Dashed straight lines represent the Arrhenius law.

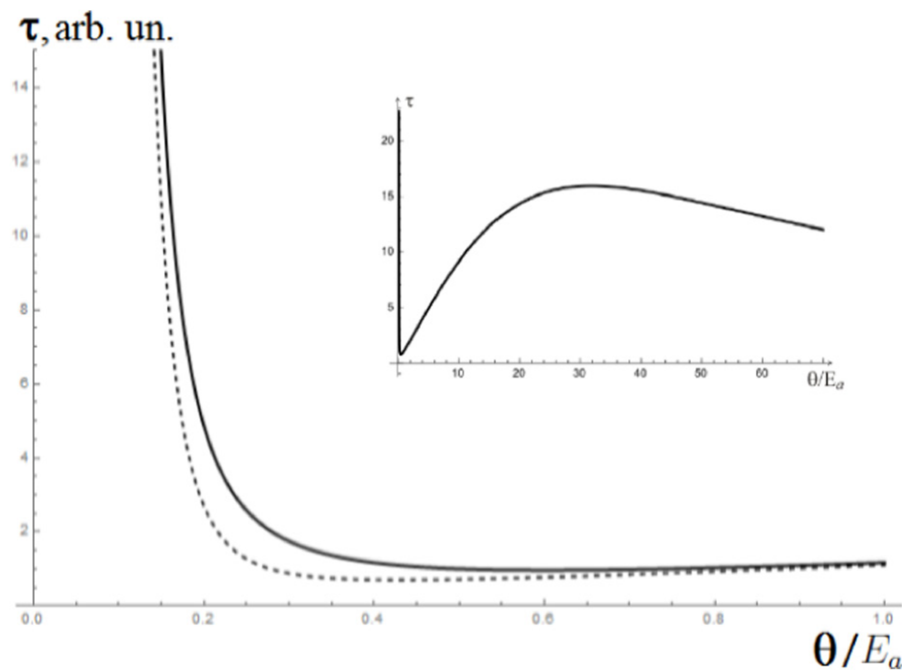

Figure 9. Relaxation time as a function of dimensionless noise intensity θ/E_a for potential profile with equal widths of barriers and wells $a = b = 0.5\ell$, where E_a is activation energy at $V = 0$ (solid line). Relaxation time for potential profile with the wide wells $a = 0.8\ell$ and narrow barriers $b = 0.2\ell$ shown in the inset in figure 2(c) (dashed line). Inset: the same relaxation time as a function of dimensionless noise intensity but for large values of θ/E_a.

J. Stat. Mech. (2020) 024003

The relaxation time (45) as a function of fluctuations intensity is shown in figure 9. The origin of fluctuations can be either thermal or from an external source. For example, the latter can be caused by a voltage driving noise added into the system. In a general case $\tau(\theta)$ is a nonmonotonic function (see the inset in figure 9). The range in which τ decreases with the intensity of the fluctuations $\theta < E_a$ is the most interesting from practical point of view, since it provides the possibility of accelerating the relaxation process through noise. As can seen from the inset of figure 9 there is an optimal value of the noise intensity so that the relaxation time is minimal.

In the case of use of the dielectric structures, with the special shapes of potential barriers and wells allowing the acceleration of diffusion (that is the nonmonotonic behavior of $D_{\text{eff}}(\theta)$ shown in figure 2), the relaxation time will become shorter. In particular, the curve with dashed line refers to a periodic potential profile with wide wells $a = 0.8\ell$ and narrow barriers $b = 0.2\ell$, while the solid line curve refers to a periodic potential profile with $a = b = 0.5$. Therefore, the choice of a particular potential profile gives rise to a further possibility of accelerating the relaxation process.

5. Conclusions

We have proposed a simple stochastic model for memristive systems. The model is validated experimentally and its ability to reproduce some fundamental properties of resistive switching such as the hysteresis of the $I - V$ characteristic and its dependence on the driving frequency is confirmed.

The proposed model takes fluctuation into account and allows us to obtain the exact analytic solutions for the concentration of defects, considered as an internal parameter of the system. This model paves the way to improve the theoretical techniques to deeper investigate the switching dynamics of the memristor devices. The steady states of the model systems are shown to be of equilibrium or nonequilibrium depending on the boundary conditions, which in turn depend on the materials of the electrodes. The nonstationary function obtained $n_1(x,t)$ provides a simplified description of transient processes within the memristive system, under arbitrary values of noise intensity, driving voltage and other parameters.

The relaxation time to the stationary state is obtained in analytic form and it has a nonmonotonic dependence on the intensity of the fluctuations for a certain set of values of the external parameters. There is an optimal intensity of external noise so that the relaxation time is minimal. Some specific shapes of potential profiles, that describe the internal structure of the memristive material, have been shown to accelerate the relaxation process. This paves the way to the use of noise as a control parameter for switching dynamics, and provides insight on the interplay between the properties of the dielectric structure and the switching times of the memristive devices.

Acknowledgments

This work was supported by the Government of the Russian Federation through Agreement No. 074-02-2018-330 (2).

References

[1] Chua L O 1971 Memristor the missing circuit element *IEEE Trans. Circuit Theory* **18** 507
[2] Strukov D B, Snider G, Stewart D and Williams R S 2008 The missing memristor found *Nature* **453** 80–3
[3] Prodromakis T, Toumazou C and Chua L 2012 Two centuries of memristors *Nat. Mater.* **11** 478–81
[4] Johnsen G K 2012 An introduction to the memristor? A valuable circuit element in bioelectricity and bioimpedance *J. Electr. Bioimpedance* **3** 20–8
[5] Waser R and Aono M 2007 Nanoionics-based resistive switching memories *Nat. Mater.* **6** 833–40
[6] Yang J J, Strukov D B and Stewart D R 2013 Memristive devices for computing *Nat. Nanotechnol.* **8** 13–24
[7] Ielmini D and Waser R 2015 *Resistive Switching: from Fundamentals of Nanoionic Redox Processes to Memristive Device Applications* (New York: Wiley)
[8] Choi B J *et al* 2016 High-speed and low-energy nitride memristors *Adv. Funct. Mater.* **26** 5290–6
[9] Li C *et al* 2018 Efficient and self-adaptive *in situ* learning in multilayer memristor neural networks *Nat. Commun.* **9** 2385
[10] Editorial 2018 The memristor revisited *Nat. Electron.* **1** 261
[11] Yang Y and Huang R 2018 Probing memristive switching in nanoionic devices *Nat. Electron.* **1** 274–87
[12] Cai F, Correll J M, Lee S H, Lim Y, Bothra V, Zhang Z, Flynn M P and Lu W D 2019 A fully integrated reprogrammable memristor-CMOS system for efficient multiply-accumulate operations *Nat. Electron.* **2** 290–9
[13] Marinella M J and Agarwal S 2019 Efficient reservoir computing with memristors *Nat. Electron.* **2** 437–8
[14] Moon J, Ma W, Shin J H, Cai F, Du C, Lee S H and Lu W D 2019 Temporal data classification and forecasting using a memristor-based reservoir computing system *Nat. Electron.* **2** 480–7
[15] Pankratov E L and Spagnolo B 2005 Optimization of impurity profile for p-n junction in heterostructures *Eur. Phys. J.* B **46** 15
[16] Cheng C, Li W, Wong T-L, Ho M K, Fung K K and Wang N 2011 Zn_2TiO_4–ZnO nanowire axial heterostructures formed by unilateral diffusion *J. Phys. Chem.* C **115** 78–82
[17] Strukov D B, Alibart F and Williams R S 2012 Thermophoresis/diffusion as a plausible mechanism for unipolar resistive switching in metal–oxide–metal memristors *Appl. Phys.* A **107** 509
[18] Rajendran B *et al* 2009 Dynamic resistance-a metric for variability characterization of phase-change memory *IEEE Electron Dev. Lett.* **30** 126–9
[19] Lacaita A, Redaelli A, Ielmini D, Pellizzer F, Pirovano A and Bez R 2004 Electrothermal and phase-change dynamics in chalcogenide-based memories *Proc. IEEE Int. Electron Devices Meeting* pp 911–4
[20] Yu S, Guan X and Wong H-S P 2011 On the stochastic nature of resistive switching in metal oxide RRAM: physical modeling, Monte Carlo simulation, and experimental characterization *Proc. IEEE Int. Electron Devices Meeting* pp 17.3.1–4
[21] Salaoru I, Khiat A, Li Q, Berdan R, Papavassiliou C and Prodromakis T 2014 Origin of the off state variability in ReRAM cells *J. Phys. D: Appl. Phys.* **47** 145102
[22] Menzel S and Waser R 2013 Analytical analysis of the generic set and reset characteristics of electrochemical metallization memory cells *Nanoscale* **5** 11003–10
[23] Suri M *et al* 2013 Bio-inspired stochastic computing using binary cbram synapses *IEEE Trans. Electron Devices* **60** 2402–9
[24] Jo S H, Kim K-H and Lu W 2008 Programmable resistance switching in nanoscale two-terminal devices *Nano Lett.* **9** 496–500
[25] Li Q, Khiat A, Salaoru I, Xu H and Prodromakis T 2014 Stochastic switching of TiO_2-based memristive devices with identical initial memory states *Nanoscale Res. Lett.* **9** 1–5
[26] Ielmini D 2016 Resistive switching memories based on metal oxides: mechanisms, reliability and scaling *Semicond. Sci. Technol.* **31** 063002
[27] Hamilton J, Afshar S, van Schaik A and Tapson J 2014 Stochastic electronics: a neuro-inspired design paradigm for integrated circuits *Proc. IEEE* **102** 843–59
[28] Naous R, Al-Shedivat M and Salama K N 2016 Stochasticity modeling in memristors *IEEE Trans. Nanotech.* **15** 15
[29] Di Ventra M 2008 *Electrical Transport in Nanoscale Systems* (Cambridge: Cambridge University Press)
[30] Yu S, Wu Y, Jeyasingh R, Kuzum D and Wong H S P 2011 An electronic synapse device based on metal oxide resistive switching memory for neuromorphic computation *IEEE Trans. Electron Devices* **58** 2729–37
[31] Sheridan P M *et al* 2017 Sparse coding with memristor networks *Nat. Nanotechnol.* **12** 784–9
[32] Yao P *et al* 2017 Face classification using electronic synapses *Nat. Commun.* **8** 15199

J. Stat. Mech. (2020) 024003

[33] Wang Z *et al* 2017 Memristor with diffusive dynamics as synaptic emulators for neuromorphic computing *Nat. Mater.* **16** 101–8
[34] Hu M *et al* 2018 Memristor-based analog computation and neural network classification with a dot product engine *Adv. Mater.* **30** 1705914
[35] Li C *et al* 2018 Analogue signal and image processing with large memristor crossbars *Nat. Electron.* **1** 52–9
[36] Hull R *et al* 2018 Stochasticity in materials structure, properties and processing—a review *Appl. Phys. Rev.* **5** 011302
[37] Chua L O and Sung M K 1976 Memristive devices and systems *Proc. IEEE* **64** 209
[38] Chua L 2018 Five non-volatile memristor enigmas solved *Appl. Phys.* A **124** 563
[39] Joglekar Y N and Wolf S J 2009 The elusive memristor: properties of basic electrical circuits *Eur J. Phys.* **30** 661
[40] Shang Y, Fei W and Yu H 2012 Analysis and modeling of internal state variables for dynamic effects of non-volatile memory devices *IEEE Trans. Circuits Syst.* **59** 1906
[41] Linn E, Siemon A, Waser R and Menzel S 2014 Applicability of well-established memristive models for simulations of resistive switching devices *IEEE Trans. Circuits Syst.* **61** 2402
[42] Ielmini D 2011 Modeling the universal set/reset characteristics of bipolar RRAM by field- and temperature-driven filament growth *IEEE Trans. Electron Devices* **58** 4309
[43] Borghetti J L, Strukov D B, Pickett M D, Yang J J and Williams R S 2009 Electrical transport and thermometry of electroformed titanium dioxide memristive switches *J. Appl. Phys.* **106** 124504
[44] Pickett D, Strukov D B, Borghetti J L, Yang J J, Snider G S, Stewart D R and Williams R S 2009 Switching dynamics in titanium dioxide memristive devices *J. Appl. Phys.* **106** 074508
[45] Kim S *et al* 2013 Physical electro-thermal model of resistive switching in bi-layered resistance-change memory *Sci. Rep.* **3** 1680
[46] Kim S, Choi S-H and Lu W 2014 Comprehensive physical model of dynamic resistive switching in an oxide memristor *ACS Nano* **8** 2369
[47] Marchewka A *et al* 2016 Nanoionic resistive switching memories: on the physical nature of the dynamic reset process *Adv. Electron. Mater.* **2** 1500233
[48] Karpov V G, Niraula D, Karpov I V and Kotlyar R 2017 Thermodynamics of phase transitions and bipolar filamentary switching in resistive random-access memory *Phys. Rev. Appl.* **8** 024028
[49] Malakhov A N and Agudov N V 1994 The kinetics of liquid-gas phase transitions of a Van der Waals substance with fluctuations taken into account *Chaos* **4** 665
[50] Valenti D, Carollo A and Spagnolo B 2018 Stabilizing effect of driving and dissipation on quantum metastable states *Phys. Rev.* A **97** 042109
[51] Carollo A, Spagnolo B and Valenti D 2018 Uhlmann curvature in dissipative phase transitions *Sci. Rep.* **8** 9852
[52] Carollo A, Spagnolo B and Valenti D 2018 Symmetric logarithmic derivative of fermionic Gaussian states *Entropy* **20** 485
[53] Stotland A and Di Ventra M 2012 Stochastic memory: memory enhancement due to noise *Phys. Rev.* E **85** 011116
[54] Jiang H *et al* 2017 A novel true random number generator based on a stochastic diffusive memristor *Nat. Commun.* **8** 882
[55] Risken H 1984 *The Fokker–Planck Equation: Methods of Solution and Applications* (Berlin: Springer)
[56] Tang S *et al* 2016 Shock waves and commutation speed of memristor *Phys. Rev.* X **6** 011028
[57] Rosenberg M J *et al* 2010 Mechanism for bipolar resistive switching in transition-metal oxides *Phys. Rev.* B **81** 115101
[58] Jo S H, Kim K-H and Lu W 2009 Programmable resistance switching in nanoscale two-terminal devices *Nano Lett.* **9** 496
[59] Medeiros-Ribeiro G *et al* 2011 Lognormal switching times for titanium dioxide bipolar memristors: origin and resolution *Nanotechnology* **22** 095702
[60] Fiasconaro A, Valenti D and Spagnolo B 2004 Nonmonotonic behavior of spatiotemporal pattern formation in a noisy Lotka–Volterra system *Acta Phys. Pol.* B **35** 1491
[61] Valenti D, Tranchina L, Brai M, Caruso A, Cosentino C and Spagnolo B 2008 Environmental metal pollution considered as noise: effects on the spatial distribution of benthic foraminifera in two coastal marine areas of sicily (Southern Italy) *Ecol. Mod.* **213** 449
[62] Chichigina O, Valenti D and Spagnolo B 2005 A simple noise model with memory for biological systems *Fluc. Noise Lett.* **5** L243
[63] Chichigina O A, Dubkov A A, Valenti D and Spagnolo B 2011 Stability in a system subject to noise with regulated periodicity *Phys. Rev.* E **84** 021134

[64] Consiglio A, Carollo A and Zenios S A 2016 A parsimonious model for generating arbitrage-free scenario trees *Quantum Financ.* **16** 201
[65] Spagnolo B, Carollo A and Valenti D 2018 Enhancing metastability by dissipation and driving in an asymmetric bistable quantum system *Entropy* **20** 226
[66] Spagnolo B, Carollo A and Valenti D 2018 Stabilization by dissipation and stochastic resonant activation in quantum metastable systems *Eur. Phys. J. Spec. Top.* **227** 379
[67] Valenti D, Magazzù L, Caldara P and Spagnolo B 2015 Stabilization of quantum metastable states by dissipation *Phys. Rev.* B **91** 235412
[68] Guarcello C, Valenti D, Augello G and Spagnolo B 2013 The role of non-Gaussian sources in the transient dynamics of long Josephson junctions *Acta Phys. Pol.* B **44** 997–1005
[69] Guarcello C, Valenti D and Spagnolo B 2015 Phase dynamics in graphene-based Josephson junctions in the presence of thermal and correlated fluctuations *Phys. Rev.* B **92** 174519
[70] Guarcello C, Valenti D, Spagnolo B, Pierro V and Filatrella G 2017 Anomalous transport effects on switching currents of graphene-based Josephson junctions *Nanotechnology* **28** 134001
[71] Guarcello C, Valenti D, Spagnolo B, Pierro V and Filatrella G 2019 Josephson-based threshold detector for Lévy-distributed current fluctuations *Phys. Rev. Appl.* **11** 044078
[72] Dubkov A A and Spagnolo B 2008 Verhulst model with Lévy noise excitation *Eur. Phys. J. B* **65** 361–7
[73] Patterson G A, Fierens P I and Grosz D F 2013 On the beneficial role of noise in resistive switching *Appl. Phys. Lett.* **103** 074102
[74] La Barbera A and Spagnolo B 2002 Spatio-temporal patterns in population dynamics *Physica* A **314** 120
[75] Valenti D, Fiasconaro A and Spagnolo B 2004 Pattern formation and spatial correlation induced by the noise in two competing species *Acta Phys. Pol.* B **35** 1481
[76] Agudov N V, Krichigin A V, Valenti D and Spagnolo B 2010 Stochastic resonance in a trapping overdamped monostable system *Phys. Rev.* E **81** 051123
[77] Tetzlaff R (ed) 2014 *Memristors and Memristive Systems* (New York: Springer)
[78] Kim W *et al* 2016 Impact of oxygen exchange reaction at the ohmic interface in Ta2O5-based ReRAM devices *Nanoscale* **41** 17774–81
[79] Ambrosi E, Bricalli A, Laudato M and Ielmini D 2019 Impact of oxide and electrode materials on the switching characteristics of oxide ReRAM devices *Faraday Discuss.* **213** 87
[80] Stratonovish R L 1963 *Topics in the Theory of Random Noise* vol 1 (New York: Gordon & Breach)
[81] Reinmann P, Van den Broeck C, Linke H, Hänggi P, Rubi J M and Perez Madrid A 2001 Giant acceleration of free diffusion by use of tilted periodic potentials *Phys. Rev. Lett.* **87** 010602
[82] Lindner B, Kotstur M and Shimansky-Geier L 2001 Optimal diffusive transport in a tilted periodic potential *Fluct. Noise Lett.* **1** R25
[83] Reimann P, Van den Broeck C, Linke H, Hänggi P, Rubi J M and Pérez-Madrid A 2002 Diffusion in tilted periodic potentials: enhancement, universality, and scaling *Phys. Rev.* E **65** 031104
[84] Agudov N and Safonov A 2005 Acceleration of diffusion in subcritically tilted periodic potentials *Fluct. Noise Lett.* **5** L283
[85] Dubkov A A and Spagnolo B 2005 Acceleration of diffusion in randomly switching potential with supersymmetry *Phys. Rev.* E **72** 041104
[86] Kulikov D, Agudov N and Spagnolo B 2011 Gaussian models for the distribution of Brownian particles in tilted periodic potentials *Eur. Phys. J.* B **83** 263
[87] Costantini G and Marchesoni F 1999 Threshold diffusion in a tilted washboard potential *Europhys. Lett.* **48** 491
[88] Filatov D *et al* 2018 Conductive atomic force microscopy study of the resistive switching in yttria stabilized zirconia films with Au nanoparticles *Scanning* **2018** 5489596
[89] Larentis S, Nardi F, Balatti S, Gilmer D C and Ielmini D 2012 Resistive switching by voltage-driven ion migration in bipolar RRAM—partII: modeling *IEEE Trans. Electr. Dev.* **59** 2468
[90] Tikhov S *et al* 2020 Electrophysical characteristics of multilayer memristive nanostructures based on yttrium stabilized zirconium dioxide and tantalum oxide *Tech. Phys.* **90** 298
[91] Mikhaylov A *et al* 2016 Field- and irradiation-induced phenomena in memristive nanomaterials *Phys. Status Solidi* **13** 870
[92] Yakimov A V *et al* 2019 Measurement of the activation energies of oxygen ion diffusion in yttria stabilized zirconia by flicker noise *Appl. Phys. Lett.* **114** 253506
[93] Ascoli A, Tetzlaff R, Chua L, Strachan J and Williams R 2016 History erase effect in a non-volatile memristor *IEEE Trans. Circuits Syst.* **63** 389

J. Stat. Mech. (2020) 024003